Macromolecules

ARTICLE

pubs.acs.org/Macromolecules

Confinement Effects of Silica Nanoparticles with Radii Smaller and Larger than R_g of Adsorbed Poly(ethylene oxide)

Rajesh Raman Madathingal and Stephanie L. Wunder*

Department of Chemistry, Temple University, Philadelphia, Pennsylvania 19122, United States

ABSTRACT: The properties of polymers on nanoparticles are different than those of the bulk, so that the interphase region becomes more important as the surface/volume ratio of the nanoparticles increases. Knowledge of the modified polymer properties is relevant both in nanocomposite applications and for nanoparticles in suspension. Polymers have chain dimensions (characterized by the radius of gyration, R_g) similar to the nanoparticles ($R_{nanoparticle}$) themselves, so that chain conformation, mobility and crystallinity can be affected by $R_g/R_{nanoparticle}$. Here, both the glass transition temperature (T_g) and degree of crystallinity (X_c) of poly(ethylene oxide) (PEO) on individual SiO_2 nanoparticles of nominal 15, 50, and 100 nm diameter ($2R_{SiO_2}$), in which R_g(PEO) was greater, equal to, or less than R_{SiO_2} was investigated. Plateau adsorption of PEO on SiO_2 nanoparticles (PEO−SiO_2) increased in the order PEO−SiO_2 (100 nm) > PEO−SiO_2 (50 nm) > PEO−SiO_2 (15 nm). At plateau adsorption, after melting and solidification, the samples were completely amorphous. The T_g of the adsorbed PEO increased in the order PEO−SiO_2 (100 nm) > PEO−SiO_2 (50 nm) > PEO−SiO_2 (15 nm); since the T_gs were above 25 °C in all cases, the PEO behaved more like a brittle solid than an elastomer. For comparable amounts of PEO that were adsorbed from solution but not melted, the melt endotherm increased in the order PEO−SiO_2 (15 nm) > PEO−SiO_2 (50 nm) > PEO−SiO_2 (100 nm). These trends were interpreted as due to an increase in loop/tail lengths and thus flexibility of the PEO chains, with a concomitant ability to crystallize, as R_g (PEO)/$R_{SiO_2\ nanoparticles}$ increased and which was the result of less hydrogen bond formation between the oxygens of PEO and the silanols (SiOH) of the SiO_2 as the nanoparticle size decreased. This in turn was attributed to the energetically unfavorable conformations necessary for the PEO chains to adopt in order to hydrogen bond with silanols on the smaller nanoparticles.

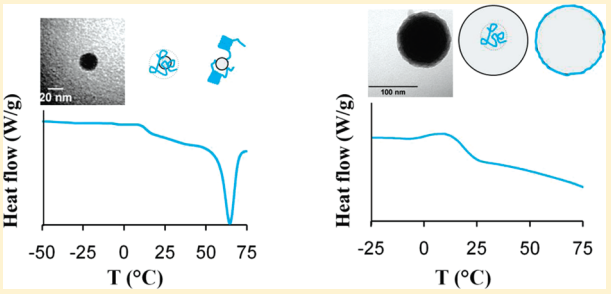

INTRODUCTION

The interaction of poly(ethylene oxide), PEO, with surfaces is important in many fields of research. It is relevant in the areas of colloid stability,[1] rheology,[2,3] biocompatible,[4] and antifouling coatings, and polymer-mediated particle synthesis, where the adsorbed polymer layer can resist compression and protein adsorption and prevent flocculation. The conformational properties of PEO with surfaces are also important for nanocomposites, in which one dimension is on the nanolength scale. Nanocomposites are often composed of a polymer matrix and a nanoparticle reinforcing agent, typically an inorganic material such as silica. The increasing use and development of nanocomposites has fostered research and engineering of the interphase region, the area over which the polymer interacts with the filler. The surface of the nanomaterial can be modified, often by chemical means such as grafting and silanization or by adsorption, to modulate polymer−particle interactions. Since the surface area in nanomaterials is large, and the effects on polymer properties have been shown to propagate considerable distances from the particle surface, the interphase region can significantly contribute to the material properties. One application of PEO nanocomposites is in lithium ion batteries, where the interaction of PEO with oxide surfaces has been investigated in charged montmorillonites[5] and has been shown to increase conductivity in the confined pores of nanoporous alumina membranes[6] and promote passivation of the lithium surface.[7] In PEO block copolymers and blends, dimensions are also in the nanoscale region, so that crystallization kinetics and morphology are affected, resulting in useful applications such as membranes that show significantly reduced oxygen permeability.[8]

There has thus been much research on the properties of polymers subjected to the effects of confinement, particularly on the glass transition temperature, T_g, in amorphous polymers,[9] and crystalline growth and lamellar morphology in semicrystalline polymers. In the case of poly(di-*n*-hexylsilane) crystallization was substantially hindered in ultrathin films, in which a critical thickness of 15 nm was needed for nucleation of crystal growth and in which the rate of crystallization was initially slow but increased rapidly as the film approached 50 nm in thickness.[10,11] T_m and T_c decreased significantly for poly[ethylene-*co*-(vinyl acetate)] below film thicknesses of 30 nm.[12] The crystallization of semicrystalline PEO has been studied in several types of confined spaces, such as diblock copolymers[13−16,17] compatible[18−21] and incompatible[8,22,23] blends,

Received: September 18, 2010
Revised: February 12, 2011
Published: March 28, 2011

networks,[24,25] thin[26,27] and ultrathin[28−30] films, pores,[6,31] nanolayer assemblies of silicates[5,32] and polymers,[8,22,23] and the surfaces of micro- and nanoparticles.[33]

The effects of confinement for PEO include an increase in the induction period for crystallization,[31] and decreases in crystallization rates,[34] melt temperatures (T_m) and enthalpies (ΔH_m or percent crystallinity).[6,24,25] The effects can be direct, for example by inhibiting sizes of crystalline domains, and indirect, by affecting T_g/mobility at the crystal/amorphous/substrate interface,[26,27,34−36] since crystallization can only occur at temperatures above T_g, where there are cooperative movements of large numbers of connected monomers. At a temperature near the average T_g of a blend of high T_g PMMA and low T_g PEO, decoupling of the local segmental dynamics of the PEO lead to confinement effects on length scales of 1 nm, where there were small PEO enclosures of high mobility in the relatively frozen PMMA matrix; at larger length scales the large scale dynamics of this fast component was strongly slowed down.[20] A similar confinement effect on small length scales was observed for PEO in a poly(vinyl acetate) blend near the T_g of the blend.[21] When confined to thicknesses of ca. 20 nm in nanolayer assemblies composed of poly(ethylene-*co*-acrylic acid) (EAA)[22] or polystyrene (PS),[8] PEO crystallized as single, very large, high-aspect-ratio lamellae, of lamellar spacing 22 nm, which resembled single crystals.

While the equilibrium structures of adsorbed polymer layers on planar surfaces are well understood,[37,38] interest in nanocomposites and colloids has motivated both theoretical and experimental work on the effects of curvature on polymer adsorption, where it is found that the key parameter that controls the influence of curvature on the structure of the interface is R/L, where R is the particle radius and L is the extension that the same layer (a layer characterized by the same loop distribution profile) would have on a flat surface.[39] Nanoparticles range from a few nm to ca. 100 nm, and thus their dimensions can be in the same size range as that of the polymers with which they are interacting. The size effect is expected to be prominent when the nanoparticle and polymer chain dimensions are comparable. Whether chain dimensions are changed by the incorporation of nanoparticles is still under debate and has recently been reviewed.[40] Experimental data for adsorption of PMMA from a good solvent onto reactive aluminum oxide (Al_2O_3) particles showed a strong dependence of adsorption on surface curvature.[41] For curved surfaces where $2R_{nanoparticle} \gg R_g$ polymer, adsorption similar to that on planar surfaces occurred. When $2R_{nanoparticle} \sim R_g$ and when $2R_{nanoparticle} \sim l_{adsorbed\ layer}$, the chains extended outward, away from the surface.[41]

In the current work, PEO of molecular weight 100 000 g/mol, with a radius of gyration (R_g) = 13.6 nm (in a Θ solvent) is adsorbed from chloroform ($CHCl_3$) onto colloidal silica (SiO_2) particles with nominal diameters of 15, 50, and 100 nm, which are in a range smaller than, comparable to, and larger than, respectively, the polymer dimensions. Adsorption isotherms are obtained to determine the amount of PEO adsorbed as a function of nanoparticle size. TEM images are used to determine whether the PEO chains form nanoparticle aggregates or adsorb to individual nanoparticles. Calorimetric and FTIR data for PEO on SiO_2 as a function of nanoparticle size provide information on the influence of loop/tail size on the glass transition and crystallization behavior of the adsorbed PEO.

EXPERIMENTAL SECTION

Materials. Poly(ethylene oxide) (PEO) with a molecular mass of 100 000 g/mol (lot no. 3001010010) was used as received (Scientific Polymer Products, Inc., Ontario, NY). Organosilicasol (colloidal silica (SiO_2)) dispersed in 2-propanol (IPA) with nominal diameters of (i) 10−15 nm, IPA-ST (30 wt % SiO_2, lot no. po601005); (ii) 40−50 nm, IPA-ST-L (30 wt % SiO_2, lot no. 160766); and (iii) 70−100 nm, IPA-ST-ZL (30 wt % SiO_2, lot no 160877) were kindly donated by Nissan Chemical America (Houston, TX) and used as received. The SiO_2 beads had densities of 2.2−2.6 g/cm^3 as reported by the manufacturer. Chloroform, $CHCl_3$ (Sigma-Aldrich, St. Louis, MO) was used as received. The properties of the SiO_2 are given in Table 1.

Table 1. Properties of Colloidal Silica in 2-propanol (IPA)

manufacturer designation	nominal diameter (nm)	diameter by TEM (nm)	diameter by DLS (nm)	ζ potential (±3 mV)[a]
ST	15	11.7 ± 2	15.2 ± 2	−40.8
ST-L	50	39.2 ± 4	46.2 ± 2	−42.0
ST-ZL	100	96.6 ± 5	102.9 ± 3	−44.2

[a] Diluted 1 IPA/100 H_2O.

Sample Preparation. PEO solutions of varying concentration were prepared in 9.3 mL chloroform. After complete dissolution of the PEO, 1 mL of colloidal SiO_2 (containing 0.3 g of SiO_2 and 0.7 mL of IPA) was added, resulting in a total solution volume of 10 mL. The colloidal silica is only available in IPA, but $CHCl_3$ is preferable for adsorption studies, since it is a noncompeting solvent for the SiO_2. The assumption is made that the small amount of IPA introduced with the SiO_2 does not affect the properties of $CHCl_3$ significantly. When dissolved even at low concentrations in IPA, PEO forms gels. The resulting mixtures were sonicated for 30 min to disperse SiO_2 in the solution. The vials were then placed in a digital vortex mixer (Fisher Scientific, Pittsburgh, PA) and mechanically agitated for 24 h at 500 rpm. The suspensions were then centrifuged at 10,000 rpm for 60 min using a Sorvall RC 5B plus centrifuge (Thomas Scientific, Swedesboro, NJ). The supernatant liquid was discarded and the SiO_2/PEO adsorbate (PEO−SiO_2) was rinsed two to three times with $CHCl_3$ to constant weight in order to remove nonadsorbed PEO. The resulting PEO−SiO_2 were dried in a vacuum oven at room temperature for 24 h and immediately stored in a desiccator. There was no residual SiO_2 in the supernatant, since centrifuge speeds and times were changed until there was only PEO in the supernatant, as assessed by TGA (weight loss is 100% for pure PEO, but does not go to 100% if SiO_2 present).

Characterization. *Adsorption Isotherms.* The amount of adsorbed PEO was measured using thermogravimetric analysis (TGA) on a TA Instruments Hi-Res TGA 2950 (TA Instruments, New Castle, DE) with a ramp rate of 10 °C/min. Samples of approximately 10−15 mg were placed in the sample pans and heated from ambient temperature to 800 °C. Nitrogen was used as a purge gas at a flow rate of 60 mL/min. In order to account for the silanol condensation of SiO_2, the beads were heated separately over the same temperature range at the same scan rate. The amount of adsorbed PEO (mg PEO/m^2 SiO_2) was obtained by subtracting the silanol weight loss from the total weight loss (silanol condensation + PEO) of the PEO−SiO_2 sample. Since small quantities of adsorbed PEO were measured, the TGA calibration was checked by thermally degrading known weights of polyethylene, with the smallest (0.8 mg) weight giving TGA losses between 100.6 and 101.2 wt %.

Characterization of SiO_2 and PEO−SiO_2 by FTIR, Calorimetry, DLS, ζ Potential, and TEM. The SiO_2 and PEO−SiO_2 were characterized by Fourier transform infrared spectroscopy (FTIR) in the transmission mode, with 256 scans and a resolution of 2 cm^{-1}, using a Mattson Research Series 1 spectrometer (Mattson Instruments, Madison, WI) equipped with a MCT detector. Samples were thinly spread on polished 32 cm sodium chloride salt plates. Dynamic light scattering (DLS) and ζ potential measurements on the SiO_2 nanoparticles were obtained on a Zeta Sizer Nano ZS (Malvern Instruments Inc., Westborough, MA). Disposable capillary cells (DTS1060) or dip cells were used for the measurement of size and ζ potentials,

respectively. All the ζ potential measurements were performed at 25 °C at electric field strengths of 3−5 V/cm, after dilution (1/100), (IPA/H_2O), from IPA, with pH values in the range of 7.1−7.5 after dilution. The reported sizes are the z-average diameters obtained by cumulant analysis.

The glass transition temperatures, T_g, melt and crystallization temperatures, T_m and T_c, and respective enthalpies, ΔH_m and ΔH_c of the PEO−SiO_2 samples were determined using a DSC 2920 (TA Instruments, New Castle, DE). To increase the sensitivity of the measurements, high volume pans (100 μL) and large sample sizes (95−100 mg) were used. The measurements were obtained at a ramp rate of 10 °C/min between −100 and +100 °C, and under a nitrogen purge at a flow rate of 60 mL/min. DSC data was obtained for three heating and cooling cycles. Repeatedly heating the samples in the DSC to 100 °C, which kept the samples above T_m for <7 min, did not change the trends in ΔH_m, T_m, or T_g. Since the trends observed for all the cycles were similar, the complete results of the second heating cycle are reported. The reverse heat flow from modulated DSC was obtained on select samples, at a heating rate of 2.5 °C/min, with an oscillation of ±1 °C for a period of 100 s.

TEM samples were prepared by placing 1 μL of SiO_2, or PEO−SiO_2 suspensions in water or ethanol, on Formvar coated copper TEM grids (Ted Pella, Inc., Redding, CA). The liquid was allowed to air-dry while holding the grid with anticapillary tweezers, leaving a thin coating of sample on the grid. The TEM analysis was performed on a FEI Technai 12T electron microscope with an operating voltage of 120 keV.

Calculation of Number of Chains/Particle. The number of PEO chains per particle, N_{PEO}/N_{SiO_2} was calculated using the following equations:

$$N_{PEO} = [m_{(PEO + SiO_2)} \cdot f_{PEO} \cdot N_A]/M_w \quad (1)$$

$$N_{SiO2} = [m_{(PEO + SiO_2)} \cdot f_{SiO_2}]/[\rho_{SiO_2}(4\pi/3)(D_{SiO_2}/2)^3] \quad (2)$$

$$\begin{aligned} N_{PEO}/N_{SiO_2} &= [f_{PEO} \cdot N_A \cdot \rho_{SiO_2} \cdot (D_{SiO_2}/2)]/[3f_{SiO_2} \cdot M_w] \\ &= \Gamma N_A 4\pi R_{SiO_2}{}^2(10^{-3}\ \mathrm{g/mg})(10^9\ \mathrm{nm/m})^2/M_w \\ &= \Gamma(\mathrm{mg/m^2})R_{SiO_2}{}^2(\mathrm{nm^2})(0.076) \end{aligned} \quad (3)$$

Here, N_A is Avogadro's number, f_{PEO} and f_{SiO_2} are the mass fractions of PMMA and SiO_2, respectively, determined from the TGA data, $m_{PEO+SiO_2}$ is the total mass of the particles after adsorption, the density of silica, $\rho_{SiO_2} = 2.2$ g/cm^3, $R_{SiO_2}(\mathrm{nm}) = D_{SiO_2}(\mathrm{nm})/2$ was taken from the TEM data for the samples, $M_w = 10^5$g/mol for PEO, and Γ is the adsorbed amount in mg/m^2.

RESULTS AND DISCUSSION

PEO of molar mass 100 000 was adsorbed onto colloidal silica nanoparticles of nominal 15, 50, and 100 nm diameter, from solutions of $CHCl_3$/2-propanol (9.3/0.7, v/v). $CHCl_3$ is a thetaΘ solvent for low molar mass PEO, and does not competitively bond to the silica surface. The 2-propanol was included since the nanoparticles were only available without a silanization agent in this solvent. An important consideration for polymer adsorption on nanoparticles is the relative size of the polymer compared with the size of the nanoparticle. If it is assumed that the $CHCl_3$/2-propanol mixture is a Θ solvent for the higher molar mass PEO, then R_g is estimated to be 13.6 nm (D = 26 nm), using $R_g = (Nb^2/6)^{1/2}$, where N is the degree of polymerization and b_{PEO} = 0.70 nm,[42] although a slightly better solvent could increase this value to at most 23.1 nm. [In a very good solvent, $r^2 = \alpha^2 r_o{}^2$, $\alpha^5 - \alpha^3 \sim M^{1/2}$; for $\alpha \gg 1$, $\alpha \sim M^{1/10}$ and therefore R_g = 23.1 nm.]. We measured a value for the hydrodynamic radius (R_H) of PEO (100 000) in IPA of 12.9 nm, so that $R_g = {}^3/_2 R_H$ = 19.4 nm. Thus, the dimensions of the PEO were larger than, comparable to and smaller than the nominal 15, 50, and 100 nm diameter SiO_2 nanoparticles, respectively, as shown schematically in Figure 1.

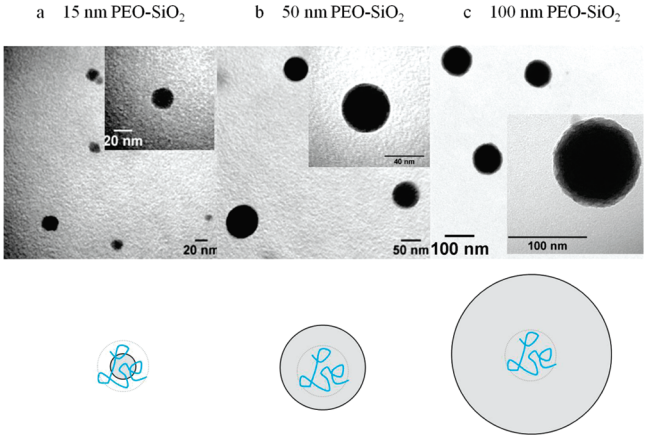

Figure 1. (Top) TEM images of nominal 15, 50, and 100 nm diameter silica nanoparticles for samples with equilibrium amounts of adsorbed PEO. (Bottom) Schematic of relative size of PEO (R_g) and $R_{nanoparticle}$ for nominal 15, 50, and 100 nm diameter silica.

The properties of the PEO/SiO_2 were investigated after adsorption from $CHCl_3$ solution and thus reflect polymer conformations in this state. The possible sites for adsorption of the PEO on the nanoparticle surface are: (i) dipole interactions of the electronegative oxygen of PEO and the silanol (SiOH) groups of silica; and (ii) much weaker hydrophobic interactions of the ethylene, $-CH_2CH_2-$, groups of PEO with the siloxane, Si−O−Si, groups of silica.[43] The stronger dipole interactions are the more likely place for PEO adsorption from $CHCl_3$ and the PEO is believed to interact with SiO_2 via an acid−base reaction in which the lone pair electrons of the ether oxygen act as the Lewis base and the surface silanols are strong Brönsted acids, resulting in hydrogen bond formation.[44]

In general, adsorbed polymer segments can be described as follows: (i) trains (segments in direct contact with surface); (ii) loops of varying size (bordered by two trains); and (iii) tails (anchored by one train).[37,38] In scaling descriptions of equilibrium polymer adsorption onto colloidal particles,[39] the adsorbed polymer has been modeled as an inner (self-similar) region made of overlapping loops and tails, surrounded by a "mushroom" region consisting of a few loops and tails that behaved as isolated chains.

The loop/tail sizes of the PEO on the adsorbed SiO_2 nanoparticles are determined by the number of segment contacts that occur as a function of nanoparticle size, and this in turn will affect both T_g and the degree of crystallization of the PEO. As discussed further below (*vida infra*), it is possible to compare the number of silanol groups/area on the silica with the number of ether oxygens of the adsorbed PEO chains (Table 2) and this can be used to make qualitative comparisons of loop sizes for PEO adsorbed onto the nominal 15, 50, and 100 nm SiO_2.

SiO_2 Nanoparticle Characterization. Since binding of PEO is affected by the surface properties of the SiO_2, the SiO_2 nanoparticles were characterized, not only for size, but also for their ζ potential values and surface silanols. The results of the TEM and ζ analysis of the particles are given in Table 1. The average ζ potential values (ξ), which were obtained in water (i.e., after a 1/100 dilution of the IPA suspension in water), become slightly more positive with decreasing bead size, suggesting

Table 2. Summary of Amount of Adsorbed PEO, Layer Thickness (h), PEO Chains/SiO_2 Nanoparticle, Oxygens/$SiOH_{iso}$, T_g, T_m, T_c, ΔH_m, and ΔH_c, for PEO on SiO_2 Nanoparticles

sample	ads. amt PEO, mg/m^2	h,[a] nm	no. of PEO chains/ SiO_2 particle	no. of O/ $SiOH_{iso}$[b]	T_m, °C	ΔH_m,[c] J/g	% cryst[d]	T_c, °C	ΔH_c,[c] J/g	T_g, °C	ΔC_p,[e] J/g°C
PEO cast from $CHCl_3$	-----				64.8	136.2	66	43.2	125.9	−50.4	0.76
PEO−SiO_2 15 nm	0.21	0.20	1.0	5.4	----	----	0	----	----	17.7	0.031
	0.28	0.27	1.3	7.2	63.9	3.6		46.9		6.7	0.034
	0.33	0.31	1.6	8.8	63.2	8.1	1.2	43.4, −32.7	2.0, 0.4	−5.6	0.041
	0.40	0.38	1.9	10.2	62.6	30.7	2.9	41.9, −35.3	5.0, 0.4	−11.7	0.017
	0.48	0.46	2.3	12.3	64.1	59.0	24.4	44.0, −31.4	47.2, 2.1	−7.8	0.020
	0.52	0.50	2.5	13.3	64.1	108.1	44.0	47.4, −32.0	87.1, 2.1	−5.8	0.028
PEO−SiO_2 50 nm	0.31	0.30	9.3	4.4	----	----	0	----	----	40.4	0.011
	0.42	0.40	12.7	6.0	----	----	0	----	----	20.9	0.025
	0.61	0.58	18.4	8.7	----	----	0	----	----	9.0	0.034
	0.64	0.61	19.3	9.2	63.4	5.3	1.3	40.1	2.4	−1.2	0.021
	0.74	0.70	22.3	10.6	62.9	14.2	3.0	43.1, −32.7	4.8, 1.4	2.4	0.053
	0.79	0.75	23.9	11.3	63.1	39.2	10.5	42.8, −33.1	13.1, 6.2	9.5	0.070
PEO−SiO_2 100 nm	0.55	0.52	84.2	6.6	----	----	0	----	----	17.6	0.016
	0.74	0.70	113	8.9	----	----	0	----	----	6.8	0.021
	0.95	0.10	145	11.4	----	----	0	----	----	3.7	0.029
	0.99	0.94	151	11.9	----	----	0	----	----	−18.9	0.016
	1.05	1.0	160	12.6	63.1	5.1	1.7	44.1	3.4	−15.1	0.015
	1.13	1.1	173	13.6	63.3	23.1	5.7	44.5	11.2	−6.7	0.024

[a] Thickness = $h = (1/\rho_{PEO})(mg_{PEO}/m_{SiO_2}{}^2)$; volume = $4\pi r_{SiO_2}{}^2 h = mass_{PEO}/\rho_{PEO}$. [b] Number of oxygen (O) adsorbed/nanobead = (O/chain) (no. of chains) = (2272.7) (no. of chains); number of isolated silanols ($SiOH_{iso}$)/nanobead = (1 $SiOH_{iso}/nm^2$) $4\pi r^2 = 4.3 \times 10^2$ (for 15 nm) = 4.8×10^3 (for 50 nm) = 2.9×10^4 (for 100 nm). [c] Normalized for wt of PEO; thus ΔH is J/g of PEO (both crystalline and amorphous), w/o weight of SiO_2. [d] Values of percent crystallinity were estimated by assuming % crystallinity = $\Delta H_m/\Delta H_m{}^o$ where $\Delta H_m{}^o$ = 205 J/g is the value for a 100% crystalline sample.[68] The value reported for the neat PEO sample was that measured for a sample crystallized from $CHCl_3$. For the PEO−SiO_2 nanocomposites, % crystallinity was further normalized for the amount of PEO (both crystalline and amorphous), without the weight of the SiO_2. [e] Corrected for amount of silica and % crystallinity; thus ΔC_p is J/g°C, where the grams are grams of amorphous PEO.

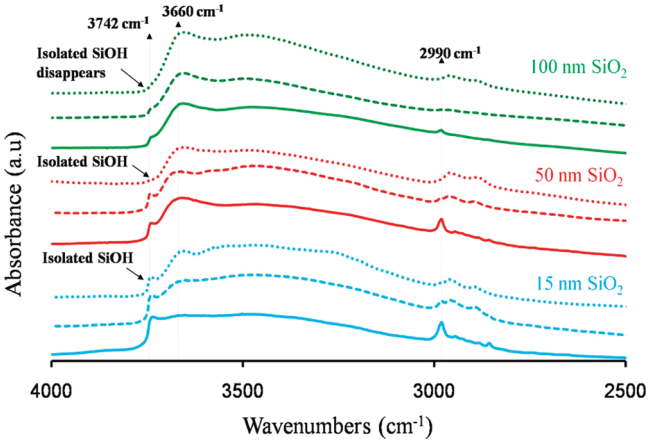

Figure 2. FTIR spectra of 15, 50 and 100 nm SiO_2 (solid lines), and with intermediate (— — —) and plateau (· · ·) adsorption amounts of PEO, all evaporated from 2-propanol. Isolated (3742 cm^{-1}), hydrogen bonded (3660 cm^{-1}) silanols and methyl/methylene vibrations (<2900 cm^{-1}) are indicated.

slightly different underlying charge densities. Previous investigations of fumed silica also have shown that the surface charge density and ζ potential increase with decreasing S_{BET}, i.e., with increasing size.[45] However, in pure 2-propanol, the surface is expected to be uncharged.

FTIR spectra provide information on the type of surface silanols on the SiO_2 nanoparticles. Figure 2 show FTIR spectra of colloidal silica with nominal 15, 50, and 100 nm diameters, evaporated from the IPA solutions. The spectra appear very similar to FTIR spectra of comparable sized beads originally in water,[46] with isolated silanol bands at 3742 cm^{-1}, hydrogen-bonded silanols at ca. 3660 cm^{-1}, inner silanols inaccessible to adsorbates between 3650−3680 cm^{-1}, and a broad water band centered at 3400 cm^{-1}. However, storage of the beads in 2-propanol results in a Si−O−$C(CH_3)_3$ bond; SiOH are known to react with alcohols such as methanol to form Si−O−C linkages.[47] The ratio of isolated to hydrogen bonded silanols, I_{3742}/I_{3660}, increases with decreasing bead size for both neat SiO_2[46] and for SiO_2 that has partially reacted with IPA.

It is not possible to obtain silanol densities for these SiO_2 particles by thermogravimetric analysis, since, despite the manufacture's indication that SiO_2 made by the water glass process should be fully condensed, the TGA weight loss of the larger beads gives physically unreasonable SiOH densities. However, the difference in the TGA data between the beads in water and in 2-propanol, when converted into "silanol densities", can be used to estimate the percentage of silanols that have reacted with 2-propanol, if it is assumed that the beads have similar silanol densities to begin with. The difference between the weight losses in the two cases can be obtained by assuming the following points: (i) 1 water molecule (MW = 18) is evolved for every 2 SiOH, or a mass of 9 is lost for every SiOH; (ii) degradation of the −C−$(CH_3)_3$ results in a weight loss of 57, possibly abstracting a hydrogen, so that the SiOH left behind can condense with another SiOH. Using these assumptions, only a small fraction of SiOH has reacted with IPA.

Although the IR spectra of the nanobeads of SiO_2 (Figure 2) are different from each other, they all have similar bands, but with different relative intensities of the isolated (3740 cm^{-1}) SiOH, hydrogen bonded/inner (3660 cm^{-1}) SiOH and water (3500 cm^{-1}) vibrations. The increased condensation observed by TGA with increasing nanoparticle size, coupled with the similar ζ potential of all size

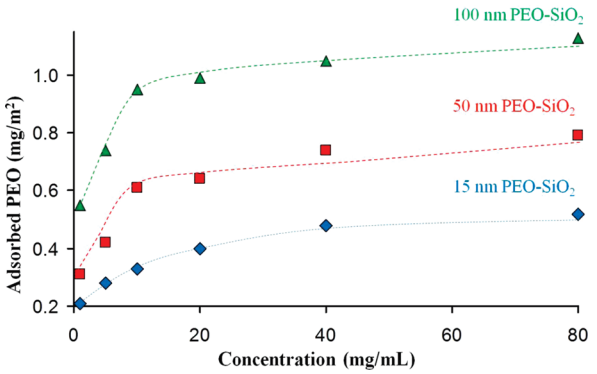

Figure 3. Adsorption isotherms for PMMA onto nominal 15, 50, and 100 nm diameter SiO_2 nanoparticles.

nanoparticles, suggests that although there is a higher proportion of uncondensed silanols in the interior of the larger nanoparticles, the surface properties are similar for all nanoparticle sizes. This surface thus is similar to that postulated for the Al_2O_3 nanoparticles, which was assumed to have the same chemical makeup for all particle sizes.[41] As was true in that case, the segment-level adsorption mechanism of hydrogen bonding interactions with SiOH (most likely isolated silanols, *vida infra*) in the current investigation is independent of surface curvature, since the monomer size of PEO (<0.5 nm) is much smaller than the smallest particle size (diameter ~15 nm) investigated.

Adsorption Isotherms of PEO onto 15, 50, and 100 nm SiO_2. Adsorption isotherms for PEO onto the nominal 15, 50, and 100 nm silica are shown in Figure 3. The isotherms are never completely flat, but change slope above a solution concentration of ca. 10 mg/mL. The slight increase in slope above a concentration of 10 mg/mL may suggest that chains not directly adsorbed to the particles become trapped by the adsorbed chains. The overlap concentration for the PEO in a Θ solvent is estimated [$C^* = (M/N_A)/({}^4/_3)\pi R_g{}^3$, M = 100 000 g/mol, and N_A = Avogadro's number] as 16.6 mg/mL. Although the nanoparticles have been rinsed three times, some entrapment may have occurred. The adsorption amounts are presented in Table 2, along with the results of calculations of the thickness of the adsorbed layer, assuming a uniform layer with the density of PEO intermediate between that of the amorphous and crystalline densities of 1.03 and 1.13 g/mol, respectively.[48] The layer thicknesses determined by TGA at plateau adsorption (ca. 0.5 to 1 nm) are consistent with values observed for other tightly bound monolayers.[49] The number of PEO chains/SiO_2 nanoparticle, calculated from eq 3 is also reported.

The results clearly show that plateau adsorption values for PEO (100 K) increased with increase in nanoparticle size, from 0.45 $mg_{PEO}/m^2{}_{SiO_2}$ for 5 nm, to 0.75 $mg_{PEO}/m^2{}_{SiO_2}$ for 50 nm, to 1 $mg_{PEO}/m^2{}_{SiO_2}$ for 100 nm SiO_2. The increase in plateau adsorption with increasing particle size has previously been observed for PEO on polystyrene lattices, where adlayer thicknesses in water doubled on 550 nm compared with 29 nm spheres,[50] and for poly(methyl methacrylate) on Al_2O_3 nanoparticles,[41] and it is predicted from theoretical models of adsorption onto colloids. The plateau adsorption values reported here for PEO on SiO_2 are consistent with those previously reported. For lower molar mass PEO (6K)[51] and PEO (7.5K and 18.5K) on 0.6, 0.86, and 1.5 μm SiO_2,[3] adsorption plateaus of 0.37 mg/m^2 and 0.35 mg/m^2, respectively, were obtained. Adsorption isotherms of PEO (600 K) on fumed silica (316 m^2/g) gave 1100 mg PEO/g SiO_2 = 0.60 mg PEO/m^2.[3,52] Values of 0.8 mg/m^2 have been reported for PEO (8×10^6) on 1 μm diameter SiO_2 with a surface area of 3.18 m^2/g.[44] In the case of PEO (10K, 100 and 600 K) values of (0.40, 0.57, and 0.74 $mg/m^2{}_{SiO_2}$), respectively, were reported for silica with a specific surface area of 17.6 m^2/g and average diameter of 0.7 μm.[53] The adsorption isotherms were less steep than the high affinity adsorption isotherms of PEO onto 1 μm diameter[44] and fumed[52] SiO_2 from water.

TEM Images of the Silica with and without Adsorbed PEO. TEM images of the silica for samples with equilibrium amounts of adsorbed PEO are presented in Figure 1. There was no difference in size for samples with or without PEO (not shown), and the PEO chains could not be observed. The images show that predominantly individual particles, and not particles entrapped in polymer or nanoparticles bridged by polymer, were obtained. Upon solvent evaporation, the particles can cluster. However, the frequency of isolated and clustered nanoparticles was similar for the bare SiO_2 and for the SiO_2 with PEO. This is in contrast to adsorption of PEO onto fumed silica, where PEO was suggested to bridge the primary particles due to the much larger size (R_g) of the PEO compared with the size of primary particles of the fumed silica.[52]

FTIR Data of PEO Adsorbed onto 15, 40, and 100 nm SiO_2. The FTIR data of PEO adsorbed onto the nominal 15, 50, and 100 nm SiO_2 for intermediate and the plateau adsorption regions are presented in Figure 2. The most dramatic change in the FTIR spectra is the decrease in intensity of the isolated silanol group vibration and relative increase in intensity of the hydrogen bonded silanols with PEO adsorption for all the nanobeads. Isolated silanols are observed for all the silica at lower amounts of adsorbed PEO, and the relative intensity of the isolated/hydrogen bonded silanols (I_{3742}/I_{3660}) decreases with increasing amount of adsorbed PEO. Further, there are differences between the 15 nm and 50/100 nm SiO_2. For the nominal 15 nm SiO_2, residual isolated silanol bands are observed at plateau adsorption, but disappear for the nominal 50 and 100 nm SiO_2.

The changes in the FTIR spectra with increasing amount of adsorbed PEO are due to the interaction of the ether oxygens of PEO with isolated silanols, resulting in a frequency shift to lower values and an intensity increase in this region as hydrogen-bonded silanols are formed. This result is consistent with isolated silanols rather than hydrogen-bonded silanols as the principal sites for adsorption or chemical reaction with adsorbates, although it is possible that the terminal SiOH in a string of H-bonded silanols also participates in PEO bonding, as has been observed for other adsorbates.[54−57] It has previously been suggested that isolated silanols are the principal sites of PEO adsorption on silica.[43,44,52]

While it is clear that hydrogen bonding of PEO to SiOH increases with PEO adsorption, it was not possible to quantify the number of ether oxygens hydrogen bonded with the isolated silanols. This is because the intensity increase is the result of both an increase in the number of H-bonded silanols with PEO adsorption, and also because the intensity of the bands is enhanced due to the increased polarity of the hydrogen bonded vibrations. The latter was demonstrated by ab initio quantum chemical calculations of a PEO fragment and a silanol group of a silica cluster, which showed enhancement of the diplole moment and intensity of the ≡SiO−H bond due to the hydrogen bonding.[52]

dx.doi.org/10.1021/ma1021693 |*Macromolecules* 2011, 44, 2873–2882

Nevertheless, it is possible to make comparisons between the three nanoparticle sizes by comparing the number of ether oxygens of PEO with the number of isolated silanols ($SiOH_{iso}$) (believed to be the sites of PEO adsorption) on the silica nanoparticles (Table 2). For PEO of MW 100 K there are 2.27×10^3 O/molecule. At plateau adsorption, there are thus 5.7×10^3, 5.4×10^4, and 3.9×10^5 oxygen atoms/nanoparticle for the 15, 50, and 100 nm SiO_2, respectively. For comparison, assuming 1 isolated $SiOH_{iso}/nm^2$, there are 3×10^2, 3.3×10^3, and 1.9×10^4 isolated silanols/nanoparticle for the 15, 50, and 100 nm SiO_2, respectively. The ratio of $O/SiOH_{isolated}$ at plateau adsorption is thus approximately the same (13, 11, and 13 for the 16, 50, and 100 nm SiO_2, respectively) for the three size nanoparticles, and there are more than sufficient oxygens in each case to hydrogen bond with all the isolated silanols. (Even if the ether oxygens could hydrogen bond with any silanol, both isolated and hydrogen bonded, and assuming 5 $SiOH/nm^2$, there would still be ca. 2.5 O/SiOH at plateau adsorption.)

However, at plateau adsorption, the isolated silanol peak completely disappears for the 100 nm SiO_2, but persists for the 15 nm SiO_2. The fact that: (i) all the isolated silanols are hydrogen bonded in the case of the 100 nm SiO_2, but residual silanols remain in the case of the 15 nm SiO_2 at plateau adsorption; and (ii) the number of $O/SiOH_{iso}$ is the approximately same for all bead sizes, means that there are a greater proportion of loops/tails for PEO on the smaller diameter nanoparticles. For the larger nanoparticles, more ether oxygens are pinned down to the silica surface, while for the smaller nanoparticles, more ether oxygens skip $SiOH_{iso}$ sites. Similarly, for comparable adsorbed amounts (Table 2), which are achieved for the 15, 50, and 100 nm SiO_2 at 0.52, 0.61, and 0.55 mg/m^2, there are 13.3, 8.7, and 6.6 $O/SiOH_{iso}$, respectively, indicating that the loop/tail size between $SiOH_{iso}$ decreases with increasing nanoparticle size.

For the 15 nm nanoparticles, only 1−2.5 chains (Table 2) adsorb to each SiO_2 nanoparticle. The lack of further hydrogen-bond formation for the adsorbed PEO chains, despite the availability of isolated silanol ($SiOH_{iso}$) sites, suggests that further hydrogen-bond formation would require that the PEO chains adopt energetically unfavorable conformations where the configurational entropy penalty was too high. This results from the small spatial extent of the nanoparticle ($R_{nanoparticle}$), compared with the dimensions of the most-probable conformation of the PEO chains (R_g), so that the PEO chain would have to become more compact than its most probable conformation in order to continue H-bond formation.

In addition, the lack of further adsorption of more PEO chains to the 15 nm nanoparticles, despite the availability of $SiOH_{iso}$ sites for adsorption, suggests that those PEO chains already on the surface are not lying flat, but are in "mushroom" conformations that have high segment densities near the surface, and large tails, preventing intrusion of incoming chains by steric repulsion. These results are consistent with theoretical models of polymers adsorbed to nanoparticles. The relative importance of the mushroom region has been shown to increase as the radius of the particle ($R_{nanoparticle}$) decreased relative to the dimensions of an adsorbed polymer of N monomers of size "a" (Kuhn length).[39] Theoretical models for which $R_{nanoparticle} < R_g$, indicate there is on average only one adsorbed polymer chain per nanoparticle, and predict self-similar monomer density profiles that extend a distance $R_{nanoparticle}$ from the surface with two large tails;[39,58] in one model, average loop lengths were insensitive to surface curvature, but tails became longer for smaller particles.[59]

By contrast, for the 100 nm SiO_2, the adsorption of PEO chains continues until all $SiOH_{iso}$ are hydrogen bonded with adsorbed or incoming PEO chains. In this case, the PEO chains H-bond with the available $SiOH_{iso}$, with less perturbation to the most probable conformation, since $R_{nanoparticle} > R_g$. Theoretical models predict a flatter polymer chain conformation in this regime. For $aN^{1/2} < R_{nanoparticle} < aN^{3/5}$, most of the adsorbed polymer is predicted to be located in the inner, self-similar region, with a few loops and tails protruding into the solution, and when $R_{nanoparticle} > aN^{3/5}$, the mushroom region vanishes, and curvature is not relevant.[39]

The results presented here are also consistent with theoretical models that consider the influence of particle size on the minimum adsorption energy per unit surface area for irreversible polymer adsorption. The adsorption energy was found to be insufficient to compensate the entropy loss on adsorption for very small particles, but adsorption on larger particles, with more adsorption sites, could take place.[60] The effect of nanoparticles on polymer chain dimensions in nanocomposites has also been considered. Although there is differing experimental evidence, for the size range investigated here, chain dimensions should either be unaffected or increased.[61]

Differential Scanning Calorimetry Data for PEO at Plateau Adsorption on 15, 40, and 100 nm SiO_2. The loop/tail size distribution resulting from the decreased number of contacts on small versus large nanoparticles (compared with R_g) has ramifications for T_g, T_m, and ΔC_p (Tables 2 and 3), as shown in Figures 4 for the nominal 15, 50, and 100 nm PEO−SiO_2. The loops/tails on the smallest bead size would be larger compared with the loops/tails on the larger size beads and thus be more mobile (decreased T_g), have more degrees of freedom (larger ΔC_p) and more easily crystallize (increased ΔH_m, X_c).

Effect of Loop/Tail Size on T_g and ΔC_p. At the lowest amounts of adsorbed PEO, only a T_g is observed for all three nanoparticle sizes. This result is in agreement with theoretical predictions indicating that flat conformations of whole chains initially adsorb,[62] and experimental ESR data for 10K spin-labeled PEO, which showed that the fraction of trains (in a system consisting of trains, loops and tails) decreased with increasing PEO concentration and contained more loops/tails as the adsorption proceeded.[53] With increasing adsorption for all the nanoparticles, the observed T_g initially decreases, suggesting that the PEO loops/tails increase in size, and thus are more flexible. At even higher adsorptions, which are a function of nanoparticle size, the loops are sufficiently large that crystallization can occur. At this point, the T_gs are observed to increase, and cold crystallization exotherms appeared, as shown in Figure 5. Modulated DSC (reversing heat flow) confirmed that the peaks seen between T_g and T_m were due to cold crystallization. The increase in T_g upon crystallization can be explained as follows: As the crystals begin to form, they grow from the highly free chains, which then no longer contribute to T_g. The chains that do contribute to T_g are therefore on average less free, so that their T_g increases. Further, as suggested from the discussion of loop/tail sizes, at comparable adsorption amounts of PEO, the smaller nanoparticles have larger loops/tails, that is, more PEO segments available for crystallization. Thus, as shown in Figure 6 for ca. 0.5−0.64 mg PEO/m^2, the melt endotherm increases in the order PEO−SiO_2 (15 nm) > PEO−SiO_2 (50 nm) > PEO−SiO_2 (100 nm); in fact at ca. 0.5 mg/nm^2, no endotherm is observed for the 100 nm SiO_2;

ΔC_ps for PEO on SiO_2 are significantly less than ΔC_p for the neat PEO, as has been previously observed,[63] and results from the restricted degrees of freedom of the PEO pinned to a solid surface. Values of ΔC_p for the PEO on all nanoparticle sizes

Table 3. Summary of Amount of Adsorbed PEO, Layer Thickness (h), PEO Chains/SiO_2 Nanoparticle, Oxygens/$SiOH_{iso}$, T_g and ΔH_c, for PEO on SiO_2 Nanoparticles Heated at 150 °C for 4 h

sample	ads. amt PEO, mg/m^2	h,[a] nm	no. of PEO chains/SiO_2 particle	no. of O/$SiOH_{iso}$[b]	T_g, °C	ΔC_p,[c] J/g°C
15 nm SiO_2	0.52	0.50	2.52	13.3	34.1	0.012
50 nm SiO_2	0.79	0.75	23.91	11.3	42.8	0.08
100 nm SiO_2	1.13	1.1	173.10	13.6	51.1	0.07

[a] Thickness = $h = (1/\rho_{PEO})(mg_{PEO}/m_{SiO_2}{}^2)$; volume $=4\pi r_{SiO_2}{}^2 h = mass_{PEO}/\rho_{PEO}$. [b] Number of oxygen (O) adsorbed/nanobead = (O/chain) (no. of chains) = (2272.7) (no. of chains) number of isolated silanols ($SiOH_{iso}$)/nanobead = (1 $SiOH_{iso}/nm^2$) $4\pi r^2 = 4.3 \times 10^2$ (15 nm); $= 4.8 \times 10^3$ (50 nm); $= 2.9 \times 10^4$ (100 nm). [c] Corrected for amount of silica and % crystallinity; thus, ΔC_p is J/g°C, where the grams are grams of amorphous PEO.

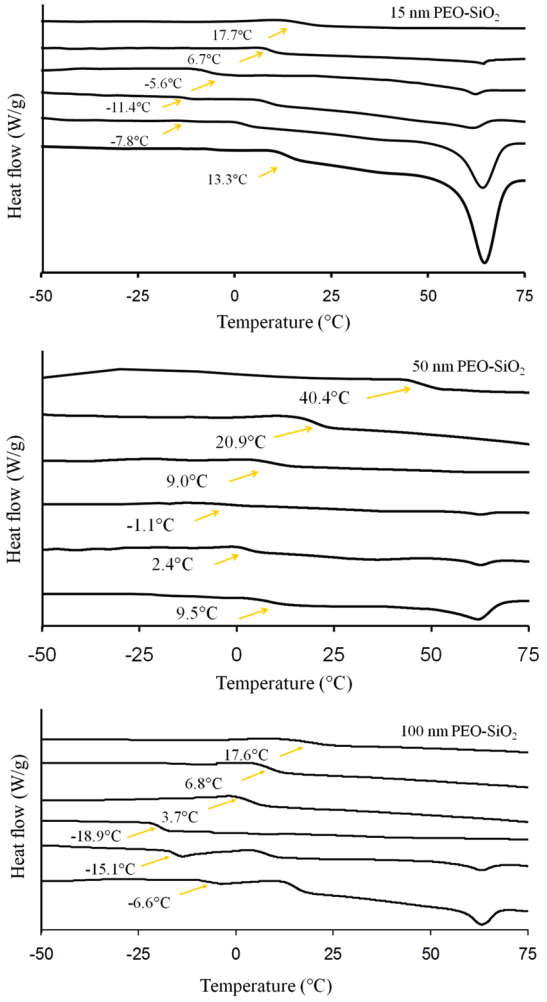

Figure 4. DSC traces for PEO adsorbed onto nominal 15 nm, 50 nm, and 100 nm SiO_2 nanoparticles as a function of increasing amount of adsorbed PEO (top to bottom) for each SiO_2 size. Arrows indicate T_gs; between T_g and T_m are small cold crystallization exotherms.

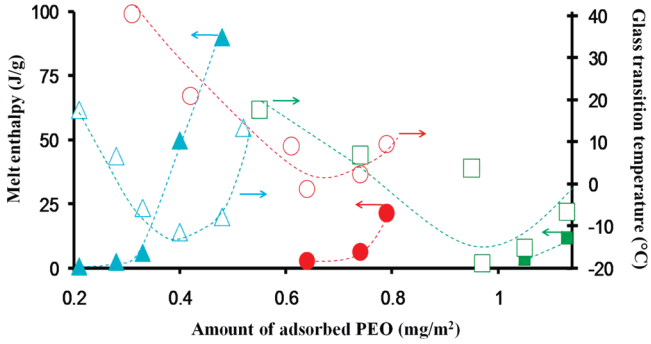

Figure 5. Melt endotherms (ΔH_m) for PEO on nominal (blue solid triangle) 15 nm, (red solid dot) 50 nm and (green solid square) 100 nm SiO_2, and T_g for PEO on nominal (blue open triangle) 15 nm, (red open dot) 50 nm and (green open square) 100 nm SiO_2, as a function of the amount of adsorbed PEO.

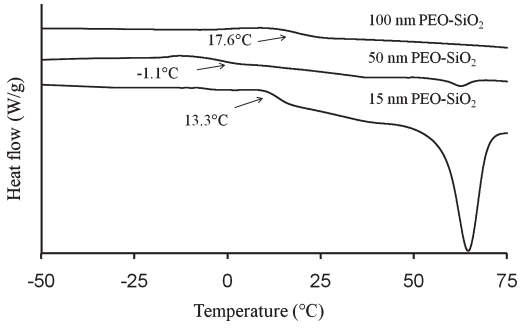

Figure 6. DSC traces of PEO adsorbed onto nominal 15, 50, and 100 nm SiO_2 nanoparticles at similar ca. 0.5−0.64 mg PEO/m^2.

increase with increase in adsorption amount. This trend is consistent with increased degrees of freedom for the PEO as more PEO is attached further from the nanoparticle surface. However, ΔC_ps also increase with decease in nanoparticle size. At plateau adsorption, ΔC_p increases in the order PEO−SiO_2 (15 nm) > PEO−SiO_2 (50 nm) > PEO−SiO_2 (100 nm). For comparable amounts of adsorbed PEO, ΔC_p increases in the order PEO−SiO_2 (15 nm) > PEO−SiO_2 (50 nm) > PEO−SiO_2 (100 nm). These trends further indicate that the loop/tail sizes are larger for PEO on the smaller nanoparticles, where the increased degrees of freedom are reflected in the higher values of the heat capacities.

Finally, samples with plateau adsorption amounts of PEO were investigated after they had been heated to 150 °C for 4 h. This thermal treatment resulted in complete disappearance of the melt endotherms. In this case, we do not know whether the PEO bridges the nanoparticles, but the disappearance of a melt suggests that the chains are too immobile to crystallize. The derivative DSC traces at plateau adsorption for the nominal 15, 50, and 100 nm PEO−SiO_2, which were heated at 150 °C for 4 h are shown in Figure 7 (data summarized in Table 3) and show that T_g decreases while ΔC_p increases for PEO as the nanoparticle size decreases, again indicating that there are fewer PEO/SiOH contacts for the smaller size nanoparticles. After melting, the −(CH_2CH_2)− groups of PEO can interact via weaker van

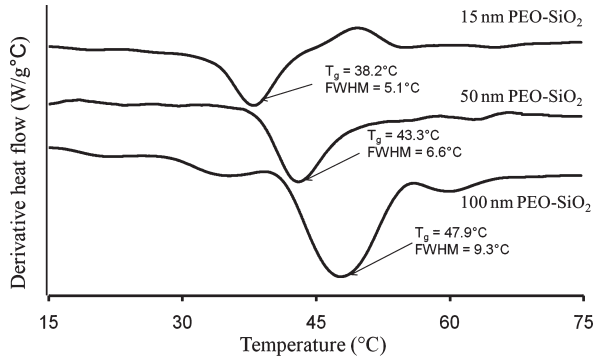

Figure 7. Derivative-DSC traces for PEO adsorbed onto nominal 15, 50, and 100 nm SiO_2 nanoparticles at plateau adsorption after heating at 150 °C for 4 h.

der Waals interactions with the Si−O−Si groups of silica, as well as through the SiOH−ether oxygen contacts discussed previously. Only a T_g is observed in this case and decreases in the order T_g (15 nm) < T_g (50 nm) < T_g (100 nm), suggesting larger loop sizes (from a smaller number of contacts), and thus greater flexibility for the smaller nanoparticles. Further, ΔC_p increases with decease in nanoparticle size for the PEO on SiO_2 heated at 150 °C/4 h, in the order ΔC_p (15 nm) > ΔC_p (50 nm) > ΔC_p (100 nm), indicating greater degrees of freedom for the PEO on the smaller nanoparticles. This trend is observed despite the much greater amount of PEO on the larger nanoparticles; T_g for polymers on attractive interfaces typically decreases with increasing adsorbed amounts.[49] The observed T_gs are 38, 43, and 48 °C for the 15, 50, and 100 nm SiO_2, respectively, and are all ca. 100 °C higher than for neat PEO (−50 °C). The T_gs are all above 25 °C, indicating that the material on the surface of the nanoparticles behaves more like a brittle solid than a flexible elastomer at room temperature.

Effect of Loop/Tail Size on Crystallization Behavior. The larger loop/tail size for the smaller nanoparticles is also manifest in the crystallization behavior. For the 15 nm SiO_2, despite the comparatively low values of adsorption/m^2, the chains crystallize, while for the 100 nm SiO_2, at adsorption amounts (ca. 0.55 mg/m^2) that are the same as for equilibrium adsorption for the 15 nm SiO_2, only a T_g is observed. The latter indicates that the PEO loops between H-bonding sites for the PEO on 100 nm SiO_2 are too short and immobile to crystallize.

T_m and T_c values for PEO on all size SiO_2 nanoparticles are almost the same as for the neat PEO, although enthalpies (and thus degrees of crystallinity) are reduced. This strongly suggests that the loop/tail lengths are sufficiently long that crystallization occurs into lamellar structures with sizes comparable to neat PEO. Since PEO lamellae of thicknesses between 8 and 20 nm have T_m of 63 °C,[23,24] lamellar thicknesses of this size must have formed on the nanoparticles; smaller thicknesses would have lower T_ms. Although the DSC data is reported for dried SiO_2−PEO constructs, it is important to remember that crystallization originally occurred from $CHCl_3$ solution, and that we are probing the properties of the solution crystallized chains.

Since it was not possible to measure the thickness (d) of the adsorbed PEO layer on SiO_2 in $CHCl_3$, due to the similarities of the refractive indices (SiO_2 = 1.46, PEO = 1.4539, $CHCl_3$ = 1.4460), we used a relationship that was developed from dynamic light scattering (DLS) data for the thickness (d) of the adsorbed layer of PEO chains on silica particles (less than 200 nm) in water, $d = 0.018M^{0.52}$. If we

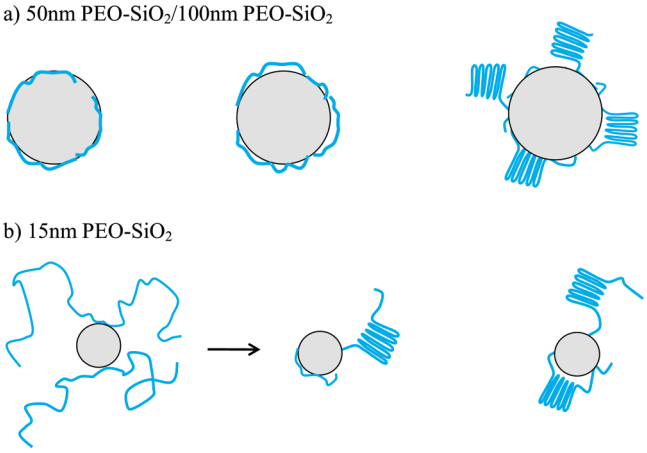

Figure 8. Schematic of (a) nominal 50 or 100 nm SiO_2 with increasing PEO adsorption, left to right; (b) nominal 15 nm SiO_2 with increasing PEO adsorption, left to right.

assume that this relationship applies for PEO in $CHCl_3$, $d \approx 7$ nm for PEO = 100 kDa. Alternatively, for grafted chains, brush heights have been shown to be comparable to ungrafted chain dimensions,[33] so that for PEO the brush heights $\approx R_g$ = 13.6−23.1 for a Θ/good solvent, respectively. Thus, when crystallization of PEO occurred for PEO tethered to the nanoparticles in solution, it was confined to a dimension of an order of magnitude between 7 and 23 nm, much larger than the thickness measured by TGA after drying. Further, the cross-sectional area of a PEO chain in a crystal lattice is 0.214 nm^2,[64] so that the crystal could only accommodate ca. 4−5 chains (1/0.214 nm) in one direction. Thus, the estimate of thickness obtained using bulk values of the density for PEO does not adequately account for the very heterogeneous nature of the PEO adsorbed onto the SiO_2 nanoparticles. The surface is most likely composed of PEO lamellae dispersed intermittently on the nanoparticles between amorphous PEO segments or bare silica.

If we consider PEO crystallization onto the 15 nm SiO_2, the similarity in size between the lamellar thickness required by the measured T_ms and nanoparticle size, as well as the fact that there is only ca. 2 PEO chains/nanoparticle, suggests that the original nucleation was not on the nanoparticles, but was instead in the $CHCl_3$, with the crystallite tethered to the nanoparticle by the adsorbed PEO segments. PEO homopolymer crystallizes in a 7_2 helical structure with a chain axis repeat distance of 1.95 nm, corresponding to 0.28 nm per monomer unit,[48] with the extended chain length given by $L = lN$, where l = 0.2783 nm, and N = number of monomers.[65−67] Therefore, for PEO (100 kDa), N = 2273, L = 633 nm. If the lamellar thickness is ca. 15 nm, one PEO chain could fold at most 42 times in the crystallite, and two chains could fold 84 times, so that the cross-sectional area would be ca. 9−18 nm^2. In view of the theoretical models that suggest long polymer tails occur on nanoparticles smaller than R_g, it is plausible that the PEO segments in the middle of the chain are amorphous and anchored to the nanoparticle, and that the tails crystallize in the solution, as shown schematically in Figure 8.

■ CONCLUSIONS

Poly(ethylene oxide) (PEO) of MW = 1 × 10^5 g/mol and R_g = 13.6 nm was adsorbed onto 15, 50, and 100 diameter silica (SiO_2) nanoparticles from chloroform solution. Transmission electron microscopy (TEM) images showed that up through the

plateau region, PEO adsorbed onto isolated spheres, with no evidence of bridging or aggregation. At plateau adsorption, there were ca. 2, 24, and 170 PEO chains/nanoparticle, for the 15, 50, and 100 nm SiO_2, respectively. This indicates that it is possible to capture single molecules of PEO on isolated nanoparticles. PEO adsorption occurred through hydrogen bond formation of the ether oxygens with the isolated silanols of SiO_2. The disappearance of the isolated silanols at plateau adsorption for the large, but not the small nanoparticles, suggested that the silanols on the smaller particles were sterically prohibited to the PEO chains. In order to hydrogen bond with these silanols, the PEO chain would have had to adopt energetically unfavorable conformations where the configurational entropy penalty of formation was high. At low adsorption amounts for all sizes of SiO_2, only a T_g was observed, due to a predominance of trains of PEO segments. As the amount of adsorbed PEO increased, a melt endotherm appeared, due to the increasing number and length of loops and dangling ends. For comparable amounts of adsorbed PEO, the melt endotherm increased in the order PEO−SiO_2 (15 nm) > PEO−SiO_2 (50 nm) > PEO−SiO_2 (100 nm). This was attributed to fewer anchoring sites for the PEO on the 15 nm SiO_2, so that crystallization occurred from the larger loop/tail sizes on these smaller nanoparticles. In all cases, T_g first decreased with increasing coverage and then increased at PEO adsorption amounts where a melt endotherm first appeared. This was interpreted as due to the removal of the freer, more mobile PEO segments that crystallized from the larger loops/tails, leaving the less free PEO segments, which therefore had a higher average T_g.

AUTHOR INFORMATION

Corresponding Author
*E-mail: slwunder@temple.edu.

REFERENCES

(1) Eisenlauer, J.; Killmann, E. *J. Colloid Interface Sci.* **1980**, *74*, 108–119.
(2) Zaman, A. A. *Colloid Polym. Sci.* **2000**, *278*, 1187–1197.
(3) Zaman, A. A.; Bjelopavlic, M.; Moudgil, B. M. *J. Colloid Interface Sci.* **2000**, *226*, 290–298.
(4) Alcantar, N. A.; Aydil, E. S.; Israelachvili, J. N. *J Biomed Mater Res* **2000**, *51*, 343–351.
(5) Bujdak, J.; Hackett, E.; Giannelis, E. P. *Chem. Mater.* **2000**, *12*, 2168–2174.
(6) Bishop, C.; Teeters, D. *Electrochim. Acta* **2009**, *54*, 4084–4088.
(7) Croce, F.; Appetecchi, G. B.; Persi, L.; Scrosati, B. *Nature* **1998**, *394*, 456–458.
(8) Wang, H. P.; Keum, J. K.; Hiltner, A.; Baer, E. *Macromolecules* **2009**, *18*, 7055–7066.
(9) Forrest, J. A.; Dalnoki-Veress, K. *Adv. Colloid Interface Sci.* **2001**, *94*, 167–196.
(10) Frank, C. W.; Rao, V.; Despotopoulou, M. M.; Pease, R. F. W.; Hinsberg, W. D.; Miller, R. D.; Rabolt, J. F. *Science* **1996**, *273*, 912–915.
(11) Despotopoulou, M. M.; Miller, R. D.; Rabolt, J. F.; Frank, C. W. *J. Polym. Sci., Polym. Phys.* **1996**, *34*, 2335–2349.
(12) Kim, J. H.; Jang, J. S.; Zin, W. C. *Macromol. Rapid Commun.* **2001**, *22*, 386–389.
(13) Lotz, B.; Kovacs, A. J.; Bassett, G. A.; Keller, A. *Kolloid Z. Z. Polym.* **1966**, *209*, 115.
(14) Zhu, L.; Calhoun, B. H.; Ge, Q.; Quirk, R. P.; Cheng, S. Z. D.; Thomas, E. L.; Hsiao, B. S.; Yeh, F.; Liu, L. Z.; Lotz, B. *Macromolecules* **2001**, *34*, 1244–1251.
(15) Zhu, L.; Cheng, S. Z. D.; Calhoun, B. H.; Ge, Q.; Quirk, R. P.; Thomas, E. L.; Hsiao, B. S.; Yeh, F.; Lotz, B. *Polymer* **2001**, *42*, 5829–5839.
(16) Hong, S.; MacKnight, W. J.; Russell, T. P.; Gido, S. P. *Macromolecules* **2001**, *34*, 2876–2883.
(17) Hong, S.; Yang, L. Z.; MacKnight, W. J.; Gido, S. P. *Macromolecules* **2001**, *34*, 7009–7016.
(18) Hoffmann, C. L.; Rabolt, J. F. *Macromolecules* **1996**, *29*, 2543–2547.
(19) Wang, M. T.; Braun, H. G.; Meyer, E. *Polymer* **2003**, *44*, 5015–5021.
(20) Genix, A. C.; Arbe, A.; Alvarez, F.; Colmenero, J.; Willner, L.; Richter, D. *Phys Rev E* **2005**, 72.
(21) Tyagi, M.; Arbe, A.; Colmenero, J.; Frick, B.; Stewart, J. R. *Macromolecules* **2006**, *39*, 3007–3018.
(22) Wang, H. P.; Keum, J. K.; Hiltner, A.; Baer, E.; Freeman, B.; Rozanski, A.; Galeski, A. *Science* **2009**, *323*, 757–760.
(23) Wang, H. P.; Keum, J. K.; Hiltner, A.; Baer, E. *Macromol. Rapid Commun.* **2010**, *31*, 356–361.
(24) Jiang, S. C.; Qiao, C. D.; Tian, S. Z.; Ji, X. L.; An, L. J.; Jiang, B. Z. *Polymer* **2001**, *42*, 5755–5761.
(25) Jiang, S.; Yu, D.; Ji, X.; An, L.; Jiang, B. *Polymer* **2000**, *41*, 2041–2046.
(26) Dalnoki-Veress, K.; Forrest, J. A.; Massa, M. V.; Pratt, A.; Williams, A. *J Polym Sci Pol Phys* **2001**, *39*, 2615–2621.
(27) Ok, S.; Demirel, A. L. *J. Macromol. Sci.—Phys.* **2003**, *B42*, 611.
(28) Reiter, G.; Sommer, J. U. *Phys. Rev. Lett.* **1998**, *80*, 3771–3774.
(29) Reiter, G.; Sommer, J. U. *J. Chem. Phys.* **2000**, *112*, 4376–4383.
(30) Sommer, J. U.; Reiter, G. *J. Chem. Phys.* **2000**, *112*, 4384–4393.
(31) Filippov, A. V.; Doroginizkij, M. M.; Vartapetyan, R. S. *Magn. Reson. Imaging* **1998**, *16*, 631–633.
(32) Hackett, E.; Manias, E.; Giannelis, E. P. *Chem. Mater.* **2000**, *12*, 2161–2167.
(33) Khan, J.; Harton, S. E.; Akcora, P.; Benicewicz, B. C.; Kumar, S. K. *Macromolecules* **2009**, *42*, 5741–5744.
(34) Schonherr, H.; Frank, C. W. *Macromolecules* **2003**, *36*, 1199–1208.
(35) Waddon, A. J.; Petrovic, Z. S. *Polym J* **2002**, *34*, 876–881.
(36) Napolitano, S.; Wubbenhorst, M. *J. Phys. Chem. B* **2007**, *111*, 5775–5780.
(37) Fleer, G. J.; Stuart, M. C.; Scheutjens, K.; Cosgrove, T.; Vincent, B., *Polymers at Interfaces*; Chapman & Hall: London, 1993.
(38) Degennes, P. G. *Adv. Colloid Interface Sci.* **1987**, *27*, 189–209.
(39) Aubouy, M.; Raphael, E. *Macromolecules* **1998**, *31* (13), 4357–4363.
(40) Liu, J.; Zhang, L. Q.; Cao, D. P.; Wang, W. C. *Phys. Chem. Chem. Phys.* **2009**, *11*, 11365–11384.
(41) Hershkovits, E.; Tannenbaum, A.; Tannenbaum, R. *J. Phys. Chem. C* **2007**, *111*, 12369–12375.
(42) Chen, E. Q.; Lee, S. W.; Zhang, A. Q.; Moon, B. S.; Mann, I.; Harris, F. W.; Cheng, S. Z. D.; Hsiao, B. S.; Yeh, F. J.; von Merrewell, E.; Grubb, D. T. *Macromolecules* **1999**, *32*, 4784–4793.
(43) Rubio, J.; Kitchener, J. A. *J. Colloid Interface Sci.* **1976**, *57*, 132–142.
(44) Mathur, S.; Moudgil, B. M. *J. Colloid Interface Sci.* **1997**, *196*, 92–98.
(45) Gun'ko, V. M.; Mironyuk, I. F.; Zarko, V. I.; Voronin, E. F.; Turov, V. V.; Pakhlov, E. M.; Goncharuk, E. V.; Nychiporuk, Y. M.; Vlasova, N. N.; Gorbik, P. P.; Mishchuk, O. A.; Chuiko, A. A.; Kulik, T. V.; Palyanytsya, B. B.; Pakhovchishin, S. V.; Skubiszewska-Zieba, J.; Janusz, W.; Turov, A. V.; Leboda, R. *J. Colloid Interface Sci.* **2005**, *289*, 427–445.
(46) Ahmed, S.; Wunder, S. L. *Langmuir* **2009**, *25*, 3682–3691.
(47) Legrand, A. P., *The Surface Properties of Silicas*; John Wiley & Sons: New York, 1998.
(48) Brandrup, J.; Immergut, E. H.; Grulke, E. A., *Polymer Handbook*; Wiley-Interscience: New York, 1999.
(49) Blum, F. D.; Young, E. N.; Smith, G.; Sitton, O. C. *Langmuir* **2006**, *22*, 4741–4744.

(50) Baker, J. A.; Pearson, R. A.; Berg, J. C. *Langmuir* **1989**, *5*, 339–342.
(51) Killmann, E.; Wild, T.; Gutling, N.; Maier, H. *Colloids Surf.* **1986**, *18*, 241–259.
(52) Voronin, E. F.; Gun'ko, V. M.; Guzenko, N. V.; Pakhlov, E. M.; Nosach, L. V.; Leboda, R.; Skubiszewska-Zieba, J.; Malysheva, M. L.; Borysenko, M. V.; Chuiko, A. A. *J. Colloid Interface Sci.* **2004**, *279*, 326–340.
(53) Esumi, K.; Iitaka, M.; Koide, Y. *J. Colloid Interface Sci.* **1998**, *208*, 178–182.
(54) Hertl, W.; Hair, M. L. *J. Phys. Chem.* **1968**, *72* (13), 4676.
(55) Hair, M. L.; Hertl, W. *J. Phys. Chem.* **1969**, *73* (12), 4269.
(56) *Silanes, Surfaces, and Interfaces*; Gordon & Breach: New York, 1986.
(57) *The Surface Properties of Silicas*; Wiley: New York, 1998.
(58) Avalos, J. B.; Jihner, A.; Diez-Orrite, S. *Eur. Phys. J. E* **2006**, 305–317.
(59) Yang, S.; Yan, D. D.; Shi, A. C. *Macromolecules* **2006**, *39*, 4168–4174.
(60) Nowicki, W. *Macromolecules* **2002**, *35*, 1424–1436.
(61) Termonia, Y. *Polymer* **2009**, *50*, 1062–1066.
(62) Fleer, G. J.; Scheutjens, J. M. H. M. In *Coagulation and Flocculation. Theory and Applications*; Dobias, B., Ed.; Dekker: New York, 1993, Chapter 5.
(63) Madathingal, R. R.; Wunder, S. L. *Langmuir* **2010**, *26*, 5077–5087.
(64) Price, F. P.; Kilb, R. W. *J. Polym. Sci.* **1962**, *57*, 395.
(65) Kovacs, A. J.; Gonthier, A. *Kolloid Z. Z. Polym.* **1972**, *250*, 530.
(66) Kovacs, A. J.; Straupe, C. *Faraday Discuss.* **1979**, 225.
(67) Kovacs, A. J.; Straupe, C. *J. Cryst. Growth* **1980**, *48*, 210–226.
(68) Martuscelli, E.; Silvestre, C.; Addonizio, M. L.; Amelino, L. *Makromol. Chem.* **1986**, *187*, 1557–1571.